Zhou et al. *Microsystems & Nanoengineering* (2025)11:220
https://doi.org/10.1038/s41378-025-01087-y

Microsystems & Nanoengineering
www.nature.com/micronano

ARTICLE Open Access

High-throughput sheathless focusing and sorting of flexible microalgae in spiral-coupled contraction-expansion channels

Teng Zhou[1]✉, Zhihao Wu[1], Long Wang[1], Shicheng Wan[1], Guibiao Qian[1], Hong Yan[2], Yongbo Deng[3] and Liuyong Shi[1]

Abstract

Haematococcus pluvialis (*H. pluvialis*) is a critical natural source of astaxanthin, recognized for its potent antioxidant capacity, anti-inflammatory properties, and ability to suppress the proliferation of breast and skin cancer cells. The size difference between microalgae such as *Chlorella vulgaris* (*C. vulgaris*) and *Haematococcus pluvialis* (*H. pluvialis*), coupled with their high research value, makes size-based separation of microalgae essential for efficient extraction of valuable species and advancing directed algal evolution. In this study, we introduce an innovative method utilizing microfluidic devices that integrate spiral channels with contraction-expansion channels. We systematically examine how variables such as flow rate, cell concentration, cell size, and three distinct coupling configurations impact cell sorting. Our results highlight that each coupling configuration of the spiral and contraction-expansion channels exerts unique control over sorting performance, offering promising new approaches for optimizing microchannel design.

Introduction

In freshwater ecosystems, *Chlorella vulgaris* (*C. vulgaris*)[1–3] and *Haematococcus pluvialis* (*H. pluvialis*)[4,5] are two algae species of great research value[6,7]. *C. vulgaris* is one of the earliest algae to be utilized for protein production and remains one of the most widely cultivated species in the global microalgae industry. In contrast, *H. pluvialis* is renowned as the premier natural source of astaxanthin. Astaxanthin is a highly potent natural antioxidant with notable biological functions, including free radical scavenging, anti-aging, anti-tumor properties, and immune modulation. The separation of *C. vulgaris*, which is rich in algal protein, from *H. pluvialis*, abundant in astaxanthin, is a key area of interest in both microalgal biology and food chemistry research (Fig. 1).

Traditional microalgal cell sorting techniques[8–10] mainly include micropipette sorting, spread plate method, differential centrifugation, and flow cytometry. In freshwater systems, *C. vulgaris* and *H. pluvialis* engage in nutrient competition, and both microalgal cells are prone to forming similar green colonies, making colony differentiation challenging. To better study individual algae, it is necessary to separate these two species. However, traditional microalgal cell sorting methods have some drawbacks, such as susceptibility to environmental conditions and growth states, small differences between closely related species, slow sorting speeds, and the requirement for specialized operational skills and expensive laboratory equipment.

Various high-throughput, high-precision, and cost-effective microfluidic methods have been developed for cell separation. Some of these methods employ external physical fields, such as dielectrophoresis[11–19], magnetophoresis[20–23], and acoustophoresis[24–28]. While effective, these techniques can expose cells to additional external stimuli and often involve complex fabrication and large experimental setups. In contrast, alternative methods leverage intrinsic microchannel structures for separation, such as inertial focusing[29–35] and elastic inertial focusing[36–38]. Inertial microfluidics, unlike elastic focusing,

Correspondence: Teng Zhou (zhouteng@hainanu.edu.cn)
[1]School of Mechanical and Electrical Engineering, Hainan University, Haikou, China
[2]School of Computer Science and Technology, Hainan University, Haikou, China
Full list of author information is available at the end of the article

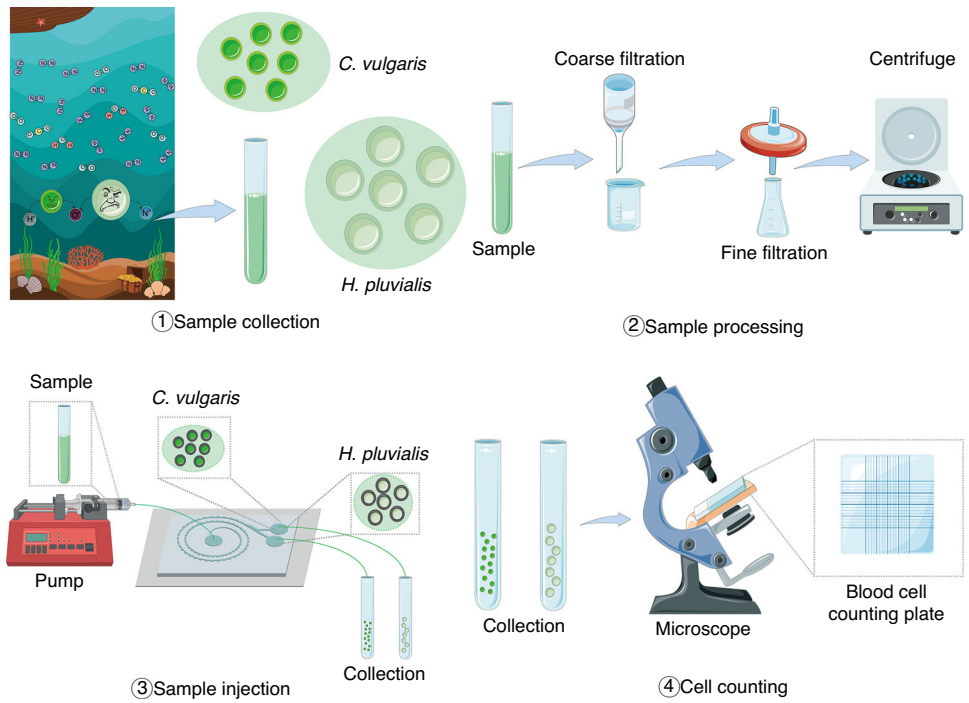

Fig. 1 Experimental Procedure Schematic The experimental procedure is divided into four specific parts, Sample Collection, Sample Processing, Sample Injection, and Cell Counting

does not rely on complex viscoelastic sample preparations or external force fields, instead utilizing microchannel design alone to achieve efficient cell sorting. In inertial focusing and sorting, particle size is a key parameter, with the critical separation threshold determined by the aspect ratio, which is the ratio between particle size and the microchannel's hydraulic diameter[39]. Inertial microfluidics[40–45] has garnered significant attention in the field of biological particle separation due to its notable advantages of simple structure, low cost, label-free operation, and high-throughput processing. Its core mechanism lies in the secondary flow induced by the channel geometry. Specifically, within the microscale flow field, the complex interplay (i.e., the hydrodynamic effect) between the inertial lift force and the Dean drag force drives particles to undergo lateral migration, ultimately focusing them at specific equilibrium positions. Within this technological framework, spiral channels are one representative structure for achieving high-throughput separation. Notably, although studies have reported that spiral channels with trapezoidal cross-sections can offer higher separation efficiency, their complex fabrication processes have limited their widespread application[46–49]. Contraction-expansion arrays (CEAs)[50,51] constitute another important class of inertial microfluidic structures. Symmetric CEA channels can achieve efficient particle separation by utilizing secondary flows induced by periodic channel variations. However, the throughput of a single symmetric CEA channel is typically lower than that of spiral channels. Therefore, achieving high-throughput separation often requires operating multiple channels in parallel. On the other hand, asymmetric CEA channels generally fail to achieve ideal separation performance without the assistance of focusing sheath flow.

Recent advances[27,52–64] in microfluidic separation have prioritized hybrid integration strategies combining inertial effects with complementary passive or active mechanisms to enhance performance metrics and application scope. The synergy between inertial prefocusing and deterministic lateral displacement (DLD) has demonstrated high-purity rare-cell isolation by merging their respective throughput and precision advantages. For instance, Nan Xiang et al.[65] developed a two-stage i-DLD chip incorporating a spiral inertial channel with DLD pillars, achieving continuous size-based separation. This design leveraged the first-stage spiral unit to remove background blood cells at high flow rates, while the second-stage triangular DLD array eliminated residual cells, yielding high-purity tumor cell recovery. Similarly, Naotomo Tottori et al.[66] implemented sheathless DLD separation by prefocusing particles along straight rectangular channels via inertial forces, eliminating dependency on sheath flows and minimizing lateral focusing length. Integration with active physical fields further enhances performance.

Concurrently, cascaded inertial architectures—such as serial spiral channels or contraction-expansion arrays (CEAs)—enable multi-step fractionation. Tatsuya Tanaka et al.[67] attained 85% recovery and 120-fold enrichment of cancer cells from RBC suspensions using a multi-stage straight-channel device, while Aynur Abdulla et al. achieved >73% accuracy for dual tumor cell types (A549/MCF-7) via cascaded spiral and zigzag channels. Hui-Sung Moon et al.[68] further demonstrated 88.8–98.9% breast cancer cell separation efficiency using a triple-stage CEA system. In contrast to modular assemblies, Al-Halhouli et al.[69] introduced embedded microcavities at spiral channel exits for enhanced spatial resolution. However, current approaches predominantly adopt modular assembly of functionally distinct units, lacking deep coupling of co-optimized channel geometries that exploit synergistic fluidic effects. Fundamental investigations into structural hybridization of co-dominant inertial mechanisms—such as integrated spiral-CEA units where Dean drag and lift forces interact constructively—remain scarce. Shahraki et al.[70] numerically demonstrated that trapezoidal spiral channels with embedded smooth or steep CEA structures can significantly enhance separation performance under idealized conditions. However, their work lacked experimental validation in biological systems, which we address through real-world testing on flexible microalgae of varying sizes. This gap impedes device miniaturization and limits performance ceilings achievable through fluid-dynamic synergy.

Herrmann et al.[71] provided a comprehensive review on spiral inertial devices for bioprocess intensification, highlighting their scalability and passive sorting advantages. Yet, few designs explored hybrid geometries or tunable structural integrations relevant to multi-species microalgal separation, particularly under dynamic growth conditions. Our prior research[35] demonstrated that effective separation between larger and smaller particles in spiral microchannels occurs only when the blockage ratio exceeds a critical threshold. For microalgae cell separation—where cellular dimensions are predetermined—the design of coupled-channel architectures must still account for this fundamental geometric constraint. However, in most existing microfluidic devices, spiral channels and contraction-expansion units have been predominantly assembled independently or implemented as repetitive modules without structural integration. Consequently, design considerations for these two distinct channel typologies are typically addressed in isolation, with minimal attention devoted to co-optimizing their parameters to achieve efficient microalgal sorting.

Magalhães et al.[72] attempted early enrichment of harmful marine microalgae using single spiral channels. While relevant for environmental sensing, their design lacked size-selectivity for heterogeneous populations and was not validated on freshwater algae such as *C. vulgaris* or *H. pluvialis*. Our novel microfluidic architecture employs global coupling of spiral and contraction-expansion units rather than conventional serial configurations, achieving enhanced Dean vorticity through abrupt cross-sectional transitions that amplify lateral migration distances of microalgae >15 μm. This contrasts with existing composite channels primarily optimized for fixed particle sizes, which lack adaptability to biological dimensional variations. Crucially, dynamic flow regulation enables real-time balance between Dean vortices and inertial lift forces, permitting continuous size-adaptive sorting throughout the microalgal growth cycle (10–25 μm). The synergistic interplay of these mechanisms establishes a tunable separation threshold unattainable in modularly assembled systems. This study introduces three novel coupling strategies that integrate spiral and contraction-expansion microfluidic channels to separate particles of varying diameters. We systematically examine how flow velocity, cell concentration, cell size, and the three coupling configurations impact cell sorting. Our findings indicate that the different coupling methods of spiral and contraction-expansion channels exhibit distinct effects on cell sorting efficiency. Building on this, the paper aims to innovate beyond existing splicing-based sorting techniques, focusing on miniaturization and achieving high-precision, sheathless, label-free microalgal cell separation using these three coupling configurations. To the best of our knowledge, this is the first report employing inertial microfluidic technology with three distinct channel coupling methods for microalgal cell sorting.

Materials and methods

Chip design and fabrication

The three coupled microchannel designs consist of a two-loop spiral microchannel integrated with three distinct types of contraction-expansion channels. The device features a single sample inlet and two outlets, with an initial spiral radius of 5 mm to ensure structural integrity. The spiral microchannel, with a rectangular cross-section, is connected to the contraction-expansion channels in three unique configurations. The width of the channels was carefully selected based on the design requirements of the contraction-expansion regions. The contraction and expansion chambers are designed with a 5° taper, and the ratio of the arc lengths of adjacent contraction and expansion chambers is approximately 1:1. As the number of loops in the Archimedean spiral increases, the arc length of the contraction-expansion chambers also grows, maintaining a consistent angular increment. The contraction chambers are designed with a width of 50 μm, while the expansion chambers are 200 μm wide. To ensure precision in fabrication, the height of the channels

is fixed at 50 μm. Thus, the contraction chamber cross-section measures 50 μm × 50 μm, and the expansion chamber cross-section measures 200 μm × 50 μm. Further details on the design process can be found in the Supporting Information, S1.

Preparation of fluorescent polystyrene microsphere samples

Fluorescent polystyrene microspheres with diameters of 5 μm and 15 μm were chosen to simulate *C. vulgaris* and *H. pluvialis*, respectively. The microspheres were suspended in ultrapure water with 1 wt% Tween-20 (Sartorius arium pro & advance) and sonicated to ensure a monodisperse suspension. The detailed design and preparation process are outlined in Supporting Information, S1.

Cell culture and sample preparation

C. vulgaris and *H. pluvialis* (in their active growth phase) were procured from Shanghai Guangyu Biological Technology Co., Ltd. and cultured under standardized conditions. *H. pluvialis* presents as motile, ellipsoidal cells, exhibiting an average maximal linear dimension of approximately 15 μm, whereas *C. vulgaris* is characterized by its more regular, spherical morphology, with a mean diameter of around 5 μm. Following initial preparation, both algal species were individually suspended in pre-formulated PBS solutions. Subsequently, the two suspensions were combined in a single test tube, thoroughly homogenized, and supplemented with sorbitol solution to facilitate subsequent experimental procedures.

Experimental procedure

The collection and preparation of both algal species were carried out first. Next, the microfluidic device was secured on a custom-made holder, and particle or cell suspensions were introduced using a syringe pump, maintaining a steady flow rate between 1 and 400 μL/min. The entire setup was placed on the stage of an inverted microscope equipped with a high-speed camera, allowing real-time monitoring and recording of the sample flow through the microchannels. Image analysis was performed using the open-access software ImageJ to overlay images, visualizing the position and trajectory of the samples. Finally, cell counting of the outlet solutions was conducted using a hemocytometer and an inverted microscope (Olympus IX73, Japan) (Fig. 1).

Analysis of focusing and separation performance

The separation efficiency is comprehensively evaluated through two principal metrics, purity (EP) and recovery rate (ER). Purity (EP) is defined as the ratio of target cells collected at outlet i to the total cellular population extracted from that specific outlet, expressed as $EP = N_a(outleti)/N_{total}(outleti)$. Recovery rate (ER) quantifies the proportion of target cells successfully retrieved from outlet i relative to the total target cells initially introduced at the inlet, calculated as $ER = N_a(outleti)/N_a(inlet)$. Given that the separation techniques based on three distinct coupled microchannel configurations are specifically designed for algal cell isolation, cell viability serves as a critical metric for analysis. To assess the viability of microalgal cells before and after separation, trypan blue staining was employed to evaluate cell health. Simultaneously, the separated microalgae were cultured for further analysis. Each test tube containing isolated algal cells was supplemented with an appropriate volume of culture medium to ensure sufficient nutrients for *C. vulgaris* and *H. pluvialis*. The microalgal suspensions collected from different outlets were incubated under initial conditions at 23°C for 7 days, with periodic shaking every hour to prevent cell sedimentation and promote uniform growth.

Results and discussion

Separation of fluorescent polystyrene microspheres in single-sided coupled spiral contraction-expansion channels

In the study of particle migration within spiral contraction-expansion single-sided coupled channels, we meticulously examined the dynamics by considering pivotal factors such as particle size and flow velocity. This analysis was instrumental in preparing the system for the separation of actual microalgal samples. We conducted an exhaustive characterization of the inertial migration within microchannels, employing fluorescent polystyrene particles that closely matched the dimensions of the target algal cells. This approach enabled a systematic evaluation of particle trajectories, which in turn allowed us to optimize the microfluidic parameters critical for subsequent biological applications. Our findings enhance the understanding of particle behavior in complex microfluidic environments. Additionally, they pave the way for more efficient microalgae separation techniques, holding significant implications for the biotechnological applications in algal research and processing.

Building on the simulation results, we carried out experimental studies to examine the inertial separation behavior of microspheres with varying diameters using optimized chip designs. The detailed simulation are outlined in Supporting Information, S1. Fluorescently labeled polystyrene microspheres were employed to facilitate clear observation of their trajectories. The particles, once focused into a single trajectory, followed an empirical relationship expressed as $a_p/h \geq 0.07$, demonstrating that the selected microspheres were capable of achieving inertial focusing and reaching a steady-state flow. To determine the optimal flow rate, we injected two types of fluorescent microspheres into the microchannels at different flow rates.

In the initial curved regions near the channel inlet, particles of varying sizes demonstrated homogeneous distribution across the cross-section without any significant focusing effect. However, as the particles navigated through the subsequent loops, they progressively converged towards their equilibrium positions. To mimic the movement of *C. vulgaris* within the microchannels, we employed fluorescent polystyrene microspheres with a diameter of 5 μm. As shown in Fig. 2, optimal focusing, characterized by single-line alignment, was achieved at flow rates of 50 μL/min, 100 μL/min, and 150 μL/min. At higher flow rates of 200 μL/min and 300 μL/min, the focusing pattern diminished, leading to a dual-line focusing phenomenon. At the flow rate of 400 μL/min, the particles failed to focus effectively, with the majority being diverted to the second outlet and a minor fraction to the first. These observations provide critical insights into the flow rate-dependent behavior of particles within the microchannels, which is essential for refining the separation process.

Utilizing the fluorescence analysis of 5 μm fluorescent polystyrene particles as a reference, we systematically varied the flow rates from 100 to 400 μL/min in increments of 100 μL/min to study the behavior of 15 μm fluorescent polystyrene particles within microchannels, thereby simulating *H. pluvialis*. As shown in Fig. 3, our experimental findings indicate that the 15 μm particles achieved precise focusing at flow rates of 100 μL/min, 200 μL/min, 300 μL/min, and 400 μL/min, culminating in a distinct single-line focus. Notably, at a flow rate of 100 μL/min, all 15 μm particles were directed to the first outlet, whereas at 200 μL/min, 300 μL/min, and 400 μL/min, the particles were consistently diverted to the second outlet. This analysis of the focusing behavior across both particle sizes suggests that the optimal flow rate for the separation of mixed particles falls within the range of 100 to 200 μL/min. The maintenance of stable equilibrium positions for the particles across a diverse array of flow rates substantiates the reliability of our device design.

Microalgae separation in spiral contraction-expansion single-side coupled channels

The focusing experiments using 5 μm and 15 μm fluorescent polystyrene particles offer valuable insights for optimizing the focusing of the two microalgae species. Unlike commercial polystyrene microspheres with consistent sizes, microalgae cells exhibit substantial size variability due to differences in growth stages and culture conditions. For instance, *H. pluvialis* can range in size from 10 μm to 25 μm. To examine the focusing behavior of the two microalgae species, individual cells were introduced into the microchannel under identical conditions, with flow rates varying from 100 μL/min to 400 μL/min.

Given the rapid growth cycle and high proliferation rate of *H. pluvialis*, we explored the impact of concentration on its focusing behavior. Detailed information regarding the concentration analysis can be found in the Supporting Information (*C. vulgaris* concentration factor section). Upon examining the focusing effects across different dilutions, we found that an 8X dilution of *H. pluvialis* exhibited a similar focusing pattern to that of 5 μm fluorescent polystyrene particles. As illustrated in Fig. 4, at a flow rate of 100 μL/min, *H. pluvialis* demonstrated effective focusing, forming a clear, single-line focus with a narrow focus width, with all particles exiting through the first outlet. At 200 μL/min, the focusing behavior shifted, resulting in bifocal flow through both outlets. A broader focus band appeared near the outer wall at the first outlet, labeled as i and ii in Fig. 4(b), while a thinner focus band formed along the inner wall at the second outlet, labeled iii. A similar bifocal pattern was observed at 300 μL/min, though the outer focus band at the first outlet became thinner (labeled i), and the inner focus band at the second outlet grew thicker (labeled ii and iii in Fig. 4(c)). At 400 μL/min, unlike the 5 μm polystyrene particles, *H. pluvialis* produced a more concentrated focus line at the first outlet, attributed to the combined effects of vortex-induced lift and Dean forces.

Based on the observed focusing behaviors of the two fluorescent polystyrene microspheres and the two microalgal species across various flow rates, mixed microalgae samples were successfully sorted. By analyzing the focusing effects of the two cell types at different flow rates, 200 μL/min was identified as the optimal flow rate for higher separation efficiency. Figure 5 illustrates Microalgae separation dynamics within spiral contraction-expansion single-side coupled microchannels. In Fig. 5(a) depicts structural overview and schematic of the spiral contraction-expansion single-side coupled microchannel, designed for efficient microalgae separation. In Fig. 5(b), the particle trajectories at the outlet of the spiral and contraction-expansion coupled microchannel are displayed, showing the clear separation of *C. vulgaris* and *H. pluvialis* into the first and second outlets, respectively. Figure 5(c) presents a grayscale image of the particle trajectories at the outlet, allowing for a quantitative analysis of the grayscale values along the M-M line from Fig. 5(b). The lateral migration of *C. vulgaris* resulted in its equilibrium position being precisely localized 96 μm from the upper boundary of the microchannel, while *H. pluvialis* achieved stable focusing at a significantly greater distance, positioned 239 μm from the same reference boundary.

In addition to visual confirmation using high-speed cameras, the performance of the spiral contraction-expansion single-side coupled sorting microchannel can also be assessed in terms of cell purity and the cells' ability

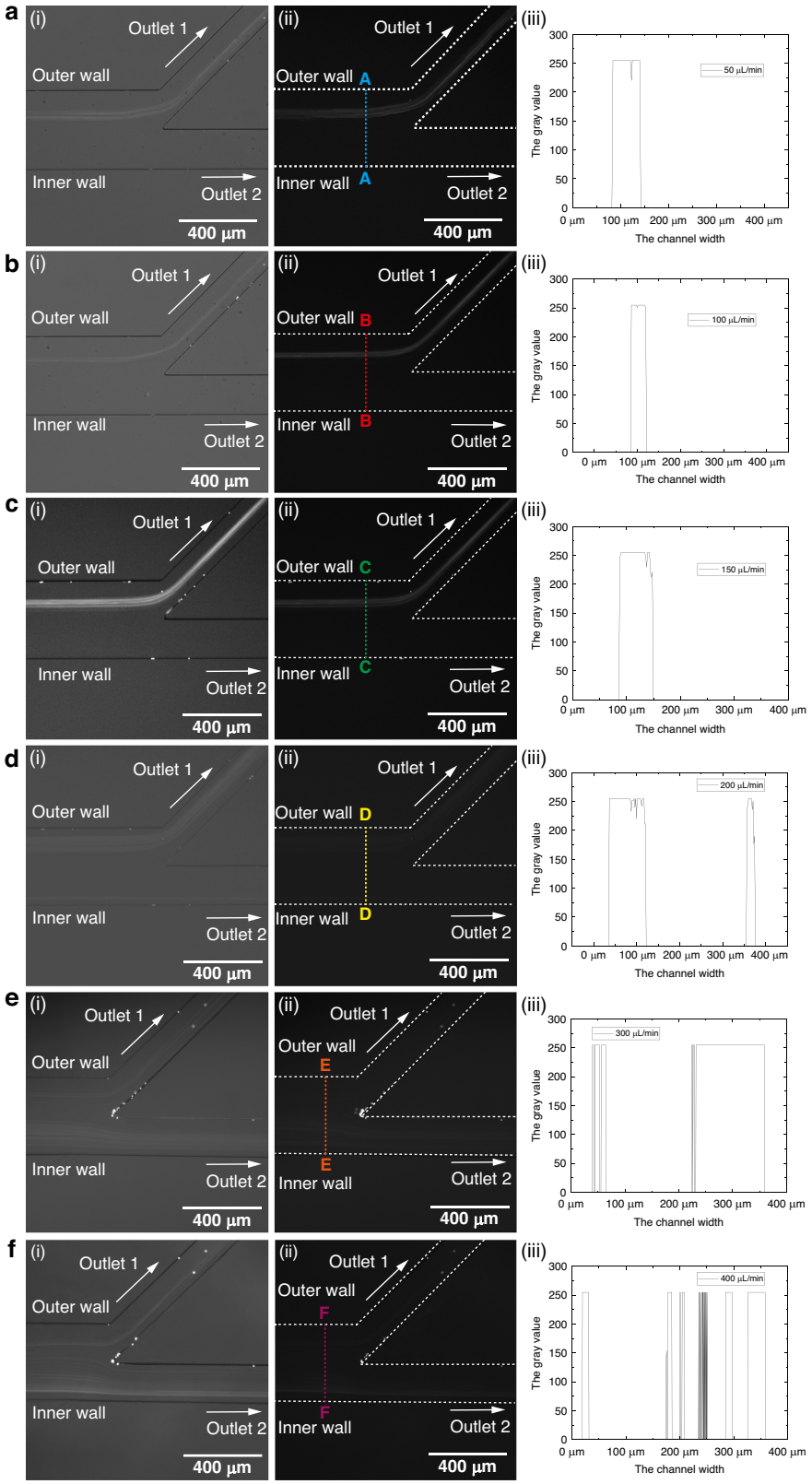

Fig. 2 Trajectories and Grayscale images of 5-μm fluorescent polystyrene microspheres at the outlet of the spiral contraction-expansion single-side coupled channel. a Flow rate of 50 μL/min, (**b**) 100 μL/min, (**c**) 150 μL/min, (**d**) 200 μL/min, (**e**) 300 μL/min, and (**f**) 400 μL/min. **i** Trajectories under bright-field imaging, (ii) trajectories under dark-field imaging, (iii) corresponding grayscale trajectory images of 5-μm fluorescent polystyrene microspheres. Scale bars: 400 μm

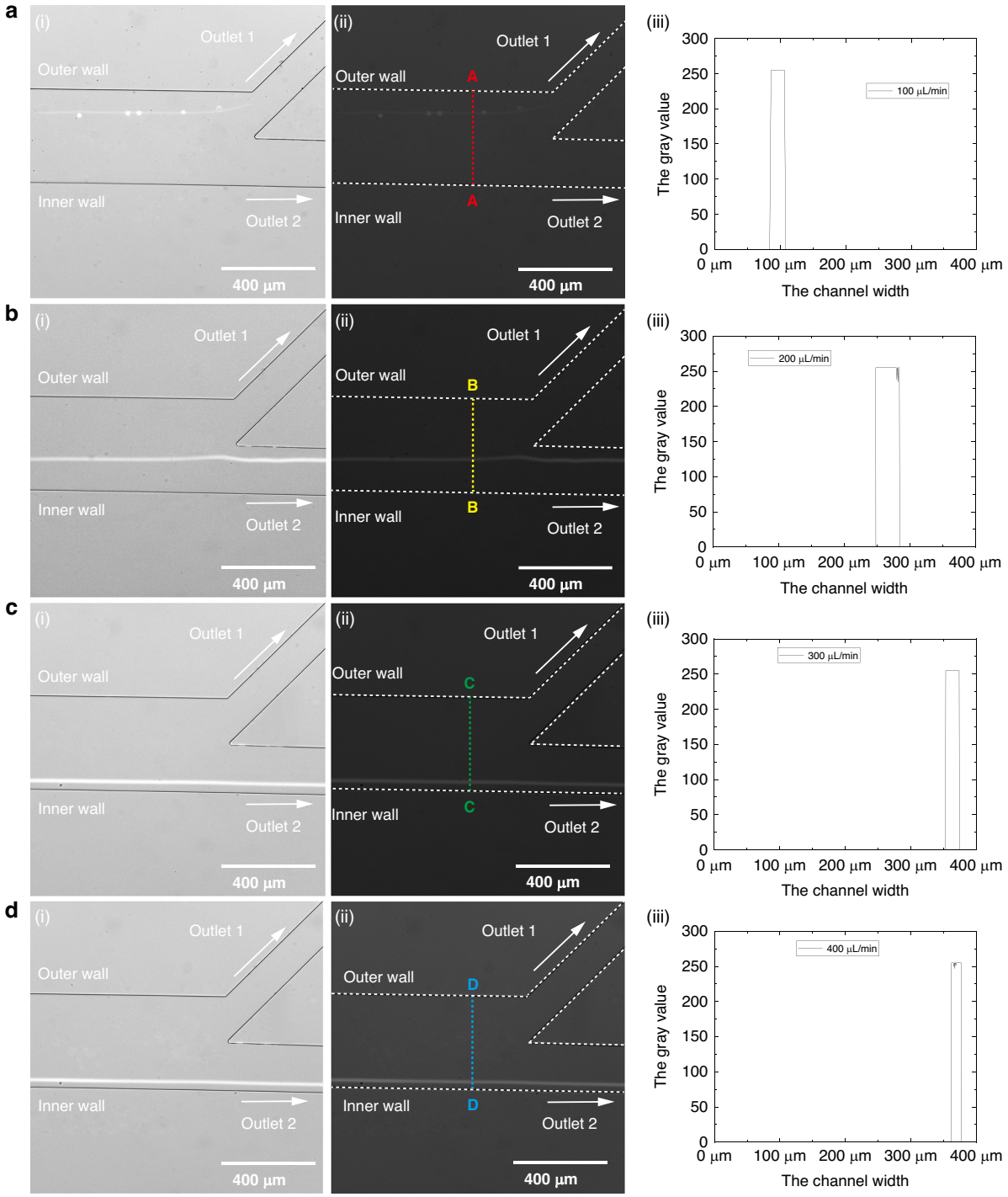

Fig. 3 Trajectories and Grayscale images of 15-μm fluorescent polystyrene microspheres at the outlet of the spiral contraction-expansion single-sided coupled channel. a Flow rate of 100 μL/min, (**b**) 200 μL/min, (**c**) 300 μL/min, (**d**) 400 μL/min. (i) Trajectories under bright-field imaging, (ii) trajectories under dark-field imaging, (iii) corresponding grayscale trajectory images of 5-μm fluorescent polystyrene microspheres. Scale bars: 400 μm

to be re-cultivated, providing practical validation of its efficacy. Under the optimized operational parameters, specifically at a flow rate of 200 μL/min, aliquots were systematically harvested from both outlets for subsequent quantitative analysis. The cellular concentrations of *C. vulgaris* and *H. pluvialis* were meticulously quantified

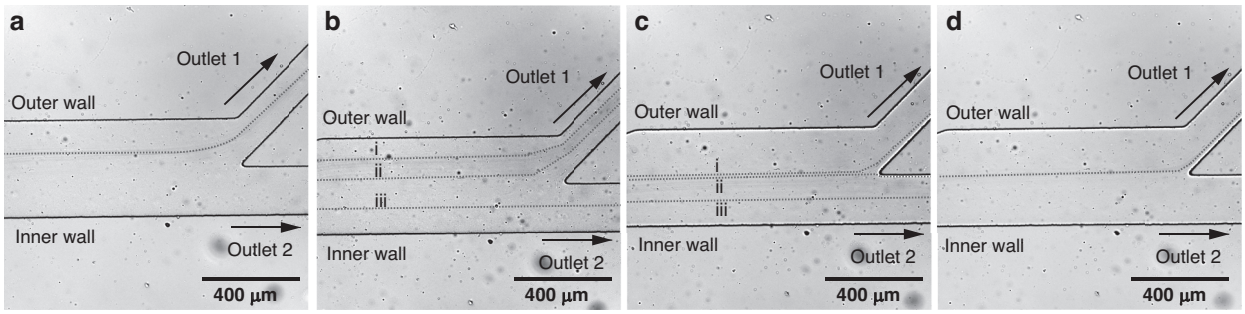

Fig. 4 Focusing of *H. pluvialis* cells diluted 8X at various flow rates in the spiral contraction-expansion single-sided coupled channel. **a** Focusing at a flow rate of 100 μL/min, (**b**) 200 μL/min, (**c**) 300 μL/min, (**d**) 400 μL/min

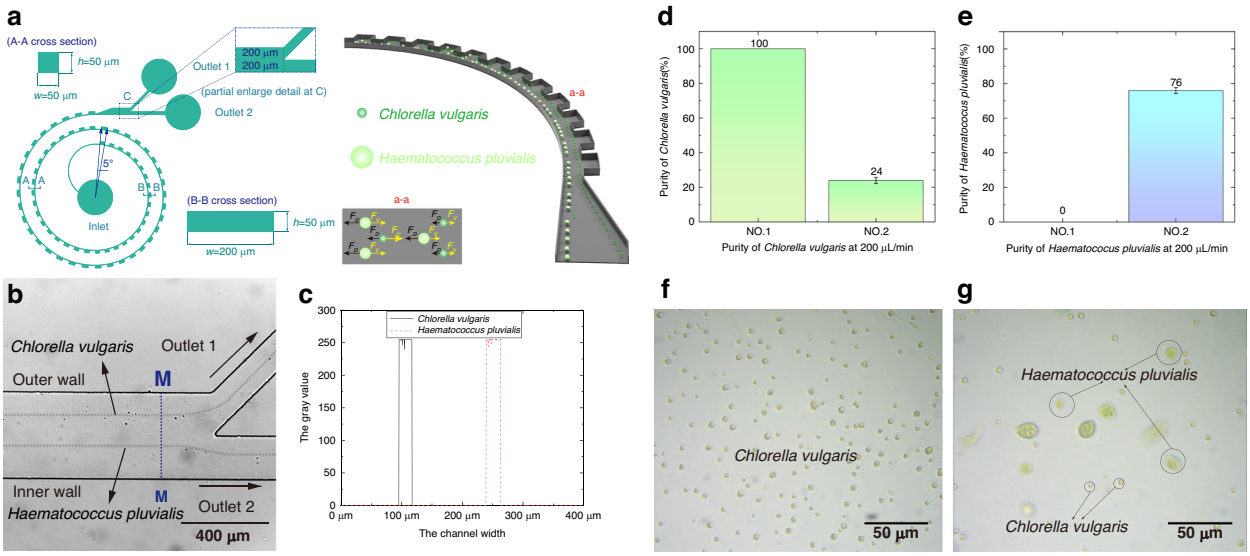

Fig. 5 Dynamics of microalgae separation in spiral contraction-expansion single-sided coupled microchannels. a Depicts the structural layout and a schematic diagram of the spiral contraction-expansion single-side coupled channel, highlighting the channel's unique design for microalgae separation. **b** Demonstrates the divergent migration pathways of assorted microalgae species, elucidating the differential behavior under the influence of the microchannel's flow dynamics. **c** Presents a grayscale image series, providing a detailed visualization of particle motion and spatial distribution along the microchannel, which is crucial for understanding the separation efficacy. **d**, **e** Quantify the purity of microalgae cells collected from each outlet at a flow rate of 200 μL/min, for *C. vulgaris* and *H. pluvialis*, respectively. **f**, **g** Display the 7-day culture results of the mixed microalgae at the two outlets of the spiral contraction-expansion single-side coupled channel, Outlet 1 and Outlet 2, respectively, illustrating the effectiveness of the separation process on the growth and purity of the cultured microalgae species

within the collected effluents, enabling precise determination of total cell counts and facilitating the assessment of microalgal purity at each respective outlet. As shown in Fig. 5(d, e), C. *vulgaris* cells collected from outlet 1 achieved a purity of 100%, while *H. pluvialis* cells from outlet 2 showed a purity of 76.5%. The lower purity at outlet 2 can be attributed to two main factors: first, some *C. vulgaris* cells adhered to the focusing pattern at outlet 2 under the 200 μL/min flow rate; second, the rapid division rate of *C. vulgaris* increased its cell concentration, which led to more particle collisions and irregular particle motion.

The single-sided coupling of the spiral and contraction-expansion channels can subject microalgal cells to considerable pressure and shear stress at high flow rates, potentially leading to cell damage. As a result, the cells' ability to regrow after separation becomes a critical performance indicator. To assess regrowth capability, separated algal cells were reseeded into fresh culture media. After 7 days of incubation, the regrowth of both *C. vulgaris* and *H. pluvialis* was observed, as depicted in Fig. 5(f) and (g). Both species showed healthy growth, with *H. pluvialis* maintaining sustained viability. The movement trails of *H. pluvialis* were clearly visible in the images, providing evidence that the cells remained undamaged during the separation process.

Following the preparation of *C. vulgaris* and *H. pluvialis* cell samples, 10 μL of each suspension was analyzed using

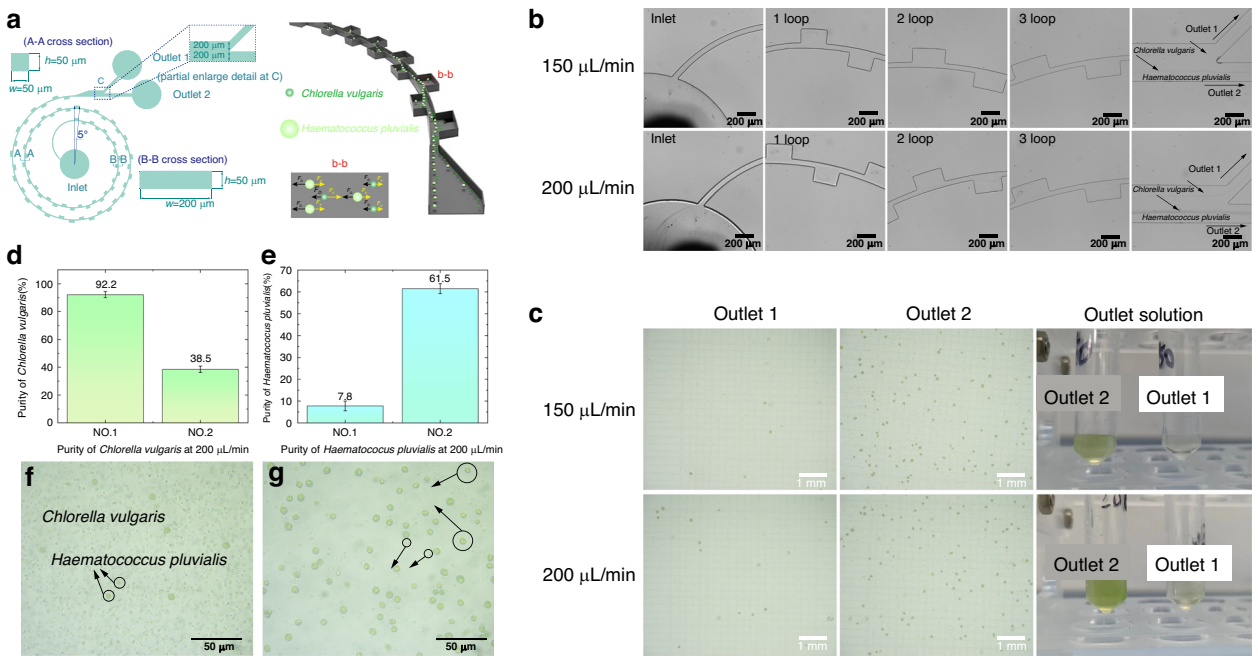

Fig. 6 Separation efficiency of microalgae in spiral contraction-expansion double-sided coupled channels. a Depicts the structural framework and a schematic diagram of the spiral contraction-expansion double-sided coupled microchannel, showcasing its innovative design for microalgae separation. **b** Presents the separation of mixed microalgae species through the channel at flow rates of 150 μL/min and 200 μL/min, demonstrating the channel's capability to discriminate between different microalgae species based on their size and inertial properties. **c** Displays the separation outcomes at the channel outlets for mixed microalgae, measured at the specified flow rates, with a focus on the efficiency and purity of the separation process. **d**, **e** Quantify the purity levels of *C. vulgaris* and *H. pluvialis*, respectively, in the collected solutions from each outlet at a flow rate of 200 μL/min, indicating the channel's effectiveness in achieving high purity separations. **f**, **g** Illustrate the 7-day cultivation results of the separated microalgae at Outlet 1 and Outlet 2 of the spiral contraction-expansion double-sided coupled microchannel, respectively, confirming the vitality and growth potential of the separated microalgae species post-separation

a hemocytometer, as shown in Figures S10(a, c). The cells were then separately stained, and after a three-minute incubation period, the samples were recounted using the hemocytometer. The post-staining results, illustrated in Figures S10(b, d), indicated a calculated cell viability of 100%. The prepared cell suspensions were subsequently introduced into the spiral contraction-expansion single-sided coupled microfluidic chip for sorting, with a flow rate set at 200 μL/min. Solutions collected from Outlets 1 and 2 were analyzed by counting 10 μL from each outlet, as sh own in Figures S11(a) and (c). Following the same staining protocol, the cells from both outlets were stained, incubated for three minutes, and then recounted. As presented in Figures S11(b, d), the results confirmed that cell purity at both outlets was within the experimental margin of error, with a calculated cell viability of 100%.

Separation of microalgae in spiral contraction-expansion double-sided coupled channel

In comparing the separation performance of *C. vulgaris* and *H. pluvialis* in a spiral contraction-expansion double-sided coupled channel with that of a single-sided coupled channel, optimal flow rates were identified as 150 μL/min and 200 μL/min. Figure 6 illustrates microalgae separation in spiral contraction-expansion double-sided coupled channels. In the Fig. 6(a), it presents the structural details and a schematic diagram of the spiral contraction-expansion double-sided coupled channel, highlighting its architecture designed for efficient microalgae separation. As shown in Fig. 6(b), at both flow rates, the mixed microalgae suspension enters the channel from the inlet in a disordered manner, subsequently traversing the first, second, and third spiral loops of the microchannel. During this passage, the two microalgae species progressively focus and begin to separate. Ultimately, *C. vulgaris* exits from the first outlet, while *H. pluvialis* exits from the second. When comparing the separation and focusing behavior at these two flow rates, it was noted that at 150 μL/min, the focusing width of *C. vulgaris* is broader than at 200 μL/min, while the focusing width of *H. pluvialis* is narrower at 150 μL/min compared to 200 μL/min.

Through collecting the solutions at the two outlets of the microchannel and performing cell counting on the outlet solutions using a blood cell counting plate and an inverted microscope, the compositions of the outlet solutions were analyzed. As shown in Fig. 6(c), the

solution at Outlet 1 mainly consisted of *C. vulgaris* and a negligible amount of *H. pluvialis*, while the solution at Outlet 2 primarily contained *H. pluvialis* with some *C. vulgaris*. The collected solution at Outlet 2 exhibited a higher concentration. Due to the bilateral coupling of the spiral and contraction-expansion channels, *C. vulgaris* were significantly affected by the vortex-induced lift force, resulting in some unstable focusing at Outlet 2. Conversely, *H. pluvialis*, impacted by the incomplete stable focusing of *C. vulgaris*, remained at Outlet 1.

Under the optimized operational conditions with a flow rate of 200 μL/min, samples were systematically collected from both Outlet 1 and Outlet 2 for subsequent quantitative assessment. By precisely measuring the concentrations of *C. vulgaris* and *H. pluvialis* within the collected effluents, the total cell count for each outlet was calculated, thereby facilitating the evaluation of algal cell purity. As illustrated in Fig. 6(d, e), the data reveal that *C. vulgaris* achieved a purity of 92.2% at Outlet 1, while *H. pluvialis* exhibited a purity of 61.5% at Outlet 2.

Similarly, in the dual-sided coupling of spiral and contraction-expansion channels, high flow rates can generate substantial pressure and shear stress in the contraction chamber, potentially leading to cell damage. To evaluate the cells' regrowth capacity post-separation, the isolated algal cells were reseeded in fresh culture medium. After 7 days of growth, the separated *C. vulgaris* and *H. pluvialis* showed healthy proliferation, confirming their viability. Notably, *H. pluvialis* displayed active movement, with clear traces of cell trajectories visible in Fig. 6(f, g), with no signs of cellular damage. Additionally, following trypan blue staining and introduction into the dual-sided microchannel chip, cell viability was confirmed to be 100%.

Separation of microalgae in spiral contraction-expansion interleaved coupled channels

Similarly, the separation of *C. vulgaris* and *H. pluvialis* in the spiral contraction-expansion interleaved coupled channel was evaluated and compared to the single-sided coupled channel. Optimal flow rates of 150 μL/min and 200 μL/min were identified for effective separation. Figure 7 illustrates microalgae separation in spiral contraction-expansion interleaved coupled channels. In the Fig. 7(a), it presents the structural composition and a schematic diagram of the spiral contraction-expansion interleaved coupled channel, outlining its innovative design for microalgae separation. As depicted in Fig. 7(b), the mixed microalgae solution entered

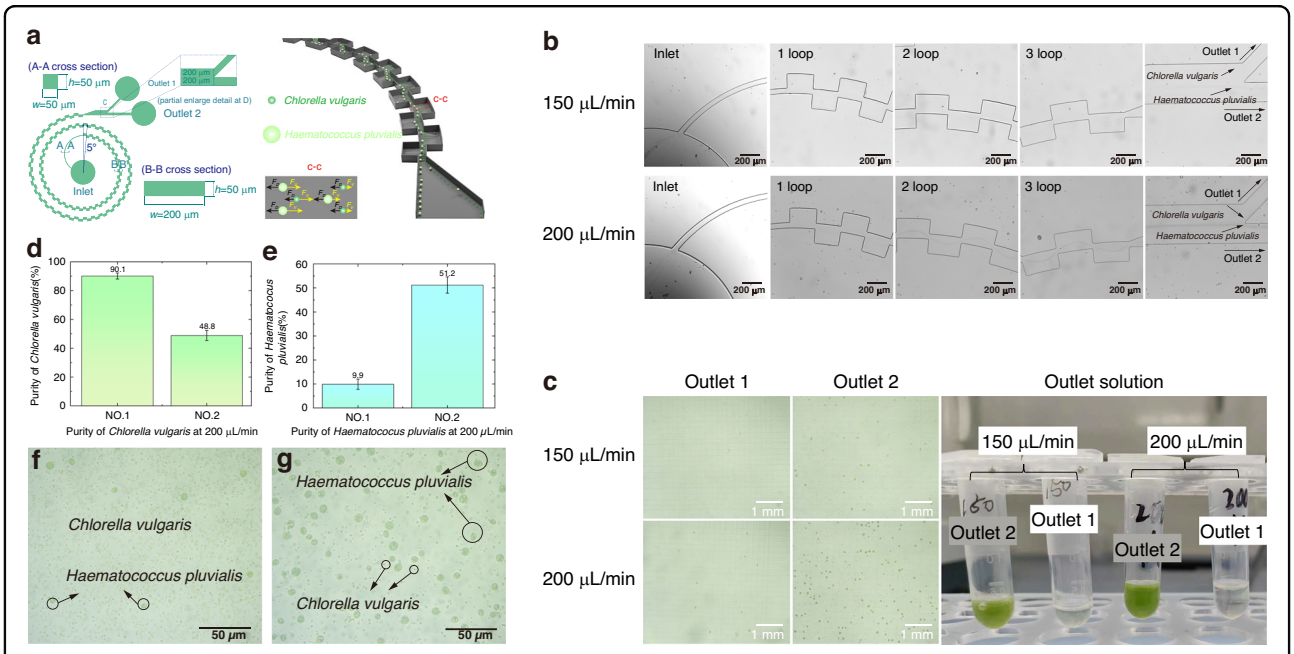

Fig. 7 Microalgae separation in spiral contraction-expansion interleaved coupled channels. a Depicts the structural composition and a schematic diagram of the spiral contraction-expansion interleaved coupled channel, outlining its innovative design for microalgae separation. **b** Demonstrates the separation effects of mixed microalgae species within the channel at flow rates of 150 μL/min and 200 μL/min, highlighting the channel's efficiency in distinguishing between different microalgae under varying flow conditions. **c** Presents the separation outcomes at the channel outlets for mixed microalgae, measured at 150 μL/min and 200 μL/min flow rates, to assess the channel's performance in fractionating microalgae species. **d** and **e** Quantify the purity of *C. vulgaris* and *H. pluvialis*, respectively, in the collected solutions from each outlet at a flow rate of 200 μL/min, indicating the precision of species separation achieved by the channel. **f** and **g** Show the 7-day cultivation results of the separated microalgae at Outlet 1 and Outlet 2 of the spiral contraction-expansion interleaved channel, respectively, validating the post-separation viability and growth of the isolated microalgae species

turbulently from the inlet and, after traversing the first, second, and third spiral loops, the two microalgae species gradually focused and separated. Ultimately, *C. vulgaris* was collected from the first outlet, while *H. pluvialis* exited from the second outlet. A comparison of the focusing and separation at both flow rates revealed that the focusing width of *C. vulgaris* remained similar. However, at 150 μL/min, the focusing position was closer to the outer wall of the channel, whereas at 200 μL/min, it shifted slightly inward. For *H. pluvialis*, the focusing width was narrower at 150 μL/min compared to 200 μL/min.

Similarly, solutions collected from the two outlets of the microchannel were analyzed using a hemocytometer and an inverted microscope for cell counting. As illustrated in Fig. 7(c), the solution from Outlet 1 primarily consists of small-sized *C. vulgaris* with a minor presence of *H. pluvialis*. Conversely, the solution from Outlet 2 predominantly contains *H. pluvialis*, along with some *C. vulgaris*. The data reveal a higher concentration of cells at Outlet 2. The interleaved coupling of the spiral and contraction-expansion channels induces significant lift forces on *C. vulgaris*, causing rapid changes in direction that lead to instability and poor focusing at Outlet 2. Consequently, some *C. vulgaris* remains unfocused and dispersed at Outlet 2, while *H. pluvialis* is retained at Outlet 1, influenced by the poorly focused *C. vulgaris*.

Under optimal conditions with a flow rate of 200 μL/min, samples were collected from both Outlet 1 and Outlet 2 for quantitative analysis. The concentrations of *C. vulgaris* and a fraction of *H. pluvialis* in the collected solutions were measured to calculate the total number of cells at each outlet, thereby determining the cell purity. As depicted in Fig. 7(d) and (e), Outlet 1 achieved a purity of 90.1% for *C. vulgaris*, whereas Outlet 2 exhibited a purity of 51.2% for *H. pluvialis*.

In the spiral and contraction-expansion channels, the alternating coupling under high flow rates subjects cells to substantial pressure and shear stress as they move through the contraction neck into the expansion chamber. This could potentially lead to cell damage. To evaluate the regrowth capability of the separated algal cells, they were reseeded into fresh culture media. As shown in Fig. 7(f) and (g), observations after 7 days of regrowth in the spiral contraction-expansion interleaved channel chip revealed strong growth for both cell types, indicating maintained viability. *H. pluvialis* demonstrated vigorous activity, with movement trails visible in the images, and no signs of cell damage were detected. Moreover, the separation process enabled the cultivation of pure single-cell cultures, achieving higher purity for individual *C. vulgaris* and *H. pluvialis* compared to conventional inertial spiral chips. The use of low-concentration algal samples optimized focusing effects, and employing natural water samples with lower algal cell densities could further enhance purity. Diluting the initial sample or conducting multiple separation rounds could also improve purity. Additionally, staining the cells with trypan blue and using the spiral contraction-expansion interleaved coupled microfluidic chip confirmed a cell viability of 100%.

Comparison of sorting performance and mechanism analysis of three coupled channels

This study reveals significant performance differences in microalgae separation using three spiral-contraction-expansion coupling strategies (single-sided, double-sided, interleaved), with separation efficiencies at 200 μL/min flow rate detailed in Table 1. These variations fundamentally stem from distinct structural designs that differentially modulate hydrodynamic behaviors. The single-sided configuration employs a terminal single contraction-expansion unit that superimposes controlled vortical forces onto the stable Dean flow field generated by the spiral channel. This design achieves 100% purity in single-stream focusing of small *C. vulgaris* cells, demonstrating optimal compatibility with the critical size threshold ($a_p/h \geq 0.07$), while attaining 76.5% purity for *H. pluvialis* with minimal vortex-induced dispersion. In contrast, although the double-sided coupling enhances transverse migration through bilateral vortices, boundary effects disrupt flow-field symmetry. This instability compromises *C. vulgaris* focusing and inversely interferes with larger cell trajectories, reducing *H. pluvialis* purity to 61.5%. The interleaved design incorporates periodically embedded contraction-expansion units (adjacent chamber arc length ratio ≈1:1), where sequential acceleration-

Table 1 Comparison of sorting performance (at a flow rate of 200 μL/min)

Coupling Configuration	Purity of *C. vulgaris*	Purity of *H. pluvialis*	Key Phenomenon
Single-sided coupling	100% (Outlet 1)	76.5% (Outlet 2)	Stable single-stream focusing of *C. vulgaris*; slight dispersion of *H. pluvialis* by vortex forces
Double-sided coupling	92.2% (Outlet 1)	61.5% (Outlet 2)	Bilateral vortices destabilize *C. vulgaris* focusing and interfere with large-cell trajectories
Interleaved coupling	90.1% (Outlet 1)	51.2% (Outlet 2)	Periodic flow perturbations displace *H. pluvialis* from equilibrium positions

deceleration cycles induce secondary flow perturbations. These perturbations destabilize equilibrium positions, particularly causing significant trajectory deviations in size-polydisperse *H. pluvialis*, further decreasing purity to 51.2%. Notably, all three configurations maintain 100% cell viability, verifying the shear-protective mechanism of microchannel designs for flexible microalgae. Regarding application efficacy, single-sided coupling emerges as the preferred approach for high-precision separation of small cells due to its structural simplicity and flow-field controllability. While double-sided and interleaved couplings enhance large-cell processing capacity through intensified vortical forces, their separation accuracy is constrained by flow-field complexity, necessitating geometric optimizations (e.g., adjusting contraction angles, chamber aspect ratios) to suppress vortex dissipation. Future work may explore hybrid coupling topologies (spiral - single-sided - interleaved sequence), where spiral zones enable pre-focusing, single-sided units achieve precise small-cell separation, and interleaved modules enrich large cells—thereby balancing efficiency and purity to establish a novel paradigm for separating biological samples with broad size distributions.

As shown in Fig. 8(a), the purity of *C.vulgaris* at Outlet 1 remained consistently high (variation <10%) as the flow rate increased from 180 to 220 μL/min, indicating robust separation stability in the single-sided coupling channel at low flow regimes. At 200 μL/min, *C.vulgaris* purity reached 100%. In contrast, the purity of *H. pluvialis* at Outlet 2 decreased significantly from ~97.1% to 70.2%, revealing reduced separation efficiency at elevated flow rates. A similar trend was observed in Fig. 8(b) for the double-sided coupling channel: *C.vulgaris* purity fluctuated minimally (<10%) around a high plateau, while *H. pluvialis* purity declined from 91.3% to 58.4%. Conversely, the interleaved coupling channel (Fig. 8c) exhibited distinct behavior: *C.vulgaris* purity increased from 87.3% to 92.6%, and *H. pluvialis* purity rose from 50.0% to 61.3% with increasing flow rate, suggesting enhanced separation efficacy under higher flow conditions.

The influence of increasing flow rate on laminar separation mechanisms varies significantly across different channel coupling configurations. In single-sided and double-sided coupling channels, at lower flow rates (<200 μL/min), the fluid exhibits stable laminar flow, facilitating efficient separation of algal particles via inertial focusing and Dean flow effects driven by size and density differences. Under these conditions, *C.vulgaris* predominantly migrates to Outlet 1 with high purity (>100%), while *H. pluvialis* is directed toward Outlet 2. However, when the flow rate increases to 220 μL/min, boundary layer instability induces intensified fluid mixing, degrading separation efficiency at Outlet 2. Concurrently, the purity of *H. pluvialis* declines markedly due to its heightened susceptibility to shear forces. In contrast, Chlorella maintains inertial stability owing to its smaller size, showing negligible purity variation.

Conversely, in interleaved coupling channels, the rapid geometric variations necessitate higher flow rates to enhance cellular focusing. Consequently, both *C.vulgaris* and *H. pluvialis* exhibit improved purity with increasing flow rates. This phenomenon correlates with local flow field gradients generated by the channel's coupled geometry, yet its core mechanism stems from flow-dependent hydrodynamic behavior, where elevated velocities optimize particle trajectory control through inertial and secondary flow interactions.

Conclusions

This study explores the separation of microalgal cells using microchannels with three distinct coupling configurations, tailored to the size of the cells. The spiral microchannel, incorporating three different periodic expansion structures, generates vortices and leverages spiral-induced lift forces. This interaction with Dean drag forces allows small particles to migrate stably

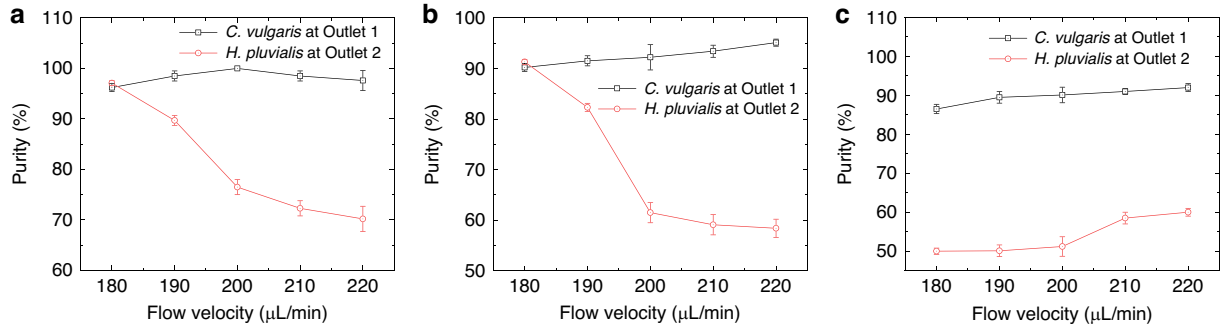

Fig. 8 Purity versus flow rate for three coupling configurations. a Single-Side Coupled Channels. **b** Double-Sided Coupled Channels. **c** Interleaved coupled channels

without being constrained by the channel geometry. In the spiral contraction-expansion single-sided coupled channel, operating at an optimal flow rate of 200 μL/min, *C. vulgaris* achieved a purity of 100%, while *H. pluvialis* reached 76.5%. For the spiral contraction-expansion double-sided coupled channel, the same flow rate yielded purities of 92.2% for *C. vulgaris* and 61.5% for *H. pluvialis*. In the spiral contraction-expansion interleaved coupled channel, *C. vulgaris* purity was 90.1% and *H. pluvialis* purity was 51.2% at 200 μL/min. Compared to conventional spiral microfluidic chips, these devices demonstrate superior performance in terms of both purity and throughput. Building on these strengths, subsequent development could focus on multi-channel array integration to substantially enhance throughput while maintaining single-channel performance. Further, integrating machine learning algorithms such as Bayesian optimization or neural networks would enable predictive modeling of the interrelationships among flow rates, channel configurations, and separation efficiency. These advances collectively pave the way for scaling this technology toward industrial-scale applications while preserving its intrinsic advantages of sheath- and label-free operation.

Acknowledgements
This research work is supported by National Natural Science Foundation of China (grant numbers 52075138, 61964006 and 62364011) and Hainan Province Science and Technology Special Fund (grant numbers ZDYF2022SHFZ301).

Author details
[1]School of Mechanical and Electrical Engineering, Hainan University, Haikou, China. [2]School of Computer Science and Technology, Hainan University, Haikou, China. [3]Institute of Microstructure Technology (IMT), Karlsruhe Institute of Technology (KIT), Eggenstein-Leopoldshafen, Germany

Author contributions
Teng Zhou: Conceptualization, Investigation, Writing –review & editing, Supervision, Funding acquisition. Zhihao Wu: Conceptualization, Methodology, Investigation, Resources, Visualization, Data curation, Writing – original draft, Writing –review & editing. Long Wang: Conceptualization, Methodology, Investigation, Resources, Writing –review & editing, Visualization. Shicheng Wan: Methodology, Investigation, Resources. Guibiao Qian: Writing –review & editing, Supervision. Hong Yan: Methodology, Investigation, Resources. Yongbo Deng: Methodology. Liuyong Shi: Writing –review & editing, Supervision, Funding acquisition.

Data availability
Data will be made available on request.

Competing interests
The author declare no competing interests.

Supplementary information The online version contains supplementary material available at https://doi.org/10.1038/s41378-025-01087-y.

Received: 22 February 2025 Revised: 15 July 2025 Accepted: 19 August 2025
Published online: 20 November 2025

References

1. Ahmad, M. T., Shariff, M., Md Yusoff, F., Goh, Y. M. & Banerjee, S. Applications of microalga in aquaculture. *Rev. Aquac.* **12**, 328–346 (2020).
2. Sepehri, A., Sarrafzadeh, M. H. & Avateffazeli, M. Interaction between and nitrifying-enriched activated sludge in the treatment of wastewater with low C/N ratio. *J. Clean. Prod.* **247**, 119164 (2020).
3. Barghchi, H. et al. The effects of Chlorella vulgaris on cardiovascular risk factors: a comprehensive review on putative molecular mechanisms. *Biomed. Pharmacother.* **162**, 114624 (2023).
4. Li, Q. et al. Chemical inducers regulate ROS signalling to stimulate astaxanthin production in Haematococcus pluvialis under environmental stresses: a review. *Trends Food Sci. Tech.* **136**, 181–193 (2023).
5. Joun, J., Sirohi, R. & Sim, S. J. The effects of acetate and glucose on carbon fixation and carbon utilization in mixotrophy of Haematococcus pluvialis. *Bioresour. Technol.* **367**, 128218 (2023).
6. Garrido-Cardenas, J. A., Manzano-Agugliaro, F., Acien-Fernandez, F. G. & Molina-Grima, E. Microalgae research worldwide. *Algal Res.* **35**, 50–60 (2018).
7. Dolganyuk, V. et al. Microalgae: a promising source of valuable bioproducts. *Biomolecules* **10**, 1153 (2020).
8. Yu, Z. et al. Droplet-based microfluidic screening and sorting of microalgal populations for strain engineering applications. *Algal Res.* **56**, 102293 (2021).
9. Ozdalgic, B. et al. Microfluidics for microalgal biotechnology. *Biotechnol. Bioeng.* **118**, 1545–1563 (2021).
10. Udayan, A., Sirohi, R., Sreekumar, N., Sang, B.-I. & Sim, S. J. Mass cultivation and harvesting of microalgal biomass: Current trends and future perspectives. *Bioresour. Technol.* **344**, 126406 (2022).
11. Lan, M. & Yang, F. Applications of dielectrophoresis in microfluidic-based exosome separation and detection. *Chem. Eng. J.* **491**, 152067 (2024).
12. Kung, Y. C., Niazi, K. R. & Chiou, P. Y. Tunnel dielectrophoresis for ultra-high precision size-based cell separation. *Lab Chip* **21**, 1049–1060 (2021).
13. Zhang, X., Xu, X., Ren, Y., Yan, Y. & Wu, A. Numerical simulation of circulating tumor cell separation in a dielectrophoresis based YY shaped microfluidic device. *Sep. Purif. Technol.* **255**, 117343 (2021).
14. Kwak, T. J., Jung, H. H., Allen, B. D., Demirel, M. C. & Chang, W. J. Dielectrophoretic separation of randomly shaped protein particles. *Sep. Purif. Technol.* **262**, 118280 (2021).
15. Wang, X. et al. Detection of prostate specific antigen in whole blood by microfluidic chip integrated with dielectrophoretic separation and electrochemical sensing. *Biosens. Bioelectron.* **204**, 114057 (2022).
16. Zhou, T. et al. Dielectrophoretic–inertial microfluidics for Symbiodinium separation and enrichment. *Phys. Fluids* **36**, 032018 (2024).
17. Zhou, T. et al. Dielectrophoretic choking phenomenon in a converging-diverging microchannel for Janus particles. *Electrophoresis* **40**, 993–999 (2019).
18. Zhou, T. et al. AC dielectrophoretic deformable particle-particle interactions and their relative motions. *Electrophoresis* **41**, 952–958 (2020).
19. Zhou, T. et al. Hydrodynamic particle focusing design using fluid-particle interactiona). *Biomicrofluidics* **7**, 054104 (2013).
20. Ruan, J. et al. A magnetophoretic microdevice for multi-magnetic particles separation based on size: a numerical simulation study. *Eng. Appl. Comp. Fluid* **16**, 1781–1795 (2022).
21. Abedini-Nassab, R., Ding, X. T. & Xie, H. Y. A novel magnetophoretic-based device for magnetometry and separation of single magnetic particles and magnetized cells. *Lab Chip* **22**, 738–746 (2022).
22. Mun, B. et al. An immuno-magnetophoresis-based microfluidic chip to isolate and detect HER2-Positive cancer-derived exosomes via multiple separation. *Biosens. Bioelectron.* **239**, 115592 (2023).
23. Giovannini, G. & De Angelis, F. Novel electro-magnetophoretic separation method for the highly sensitive detection of analytes. *Nanoscale Horiz.* **5**, 95–101 (2020).
24. Undvall Anand, E. et al. Two-step acoustophoresis separation of live tumor cells from whole blood. *Anal. Chem.* **93**, 17076–17085 (2021).
25. Olofsson, K., Hammarstrom, B. & Wiklund, M. Acoustic separation of living and dead cells using high density medium. *Lab Chip* **20**, 1981–1990 (2020).
26. Gu, Y. Y. et al. Acoustofluidic centrifuge for nanoparticle enrichment and separation. *Sci. Adv.* **7**, eabc0467 (2021).
27. Fan, Y. P., Wang, X., Ren, J. Q., Lin, F. & Wu, J. D. Recent advances in acoustofluidic separation technology in biology. *Microsyst. Nanoeng.* **8**, 94 (2022).
28. Lei, J. J., Cheng, F., Li, K. M. & Guo, Z. N. Numerical simulation of continuous separation of microparticles in two-stage acousto-microfluidic systems. *Appl. Math. Model.* **83**, 342–356 (2020).

29. Cha, H. T. et al. Tuning particle inertial separation in sinusoidal channels by embedding periodic obstacle microstructures. *Lab Chip* **22**, 2789–2800 (2022).
30. Fallahi, H., Zhang, J., Nicholls, J., Phan, H. P. & Nguyen, N. T. Stretchable inertial microfluidic device for tunable particle separation. *Anal. Chem.* **92**, 12473–12480 (2020).
31. Kim, G. Y., Son, J., Han, J. I. & Park, J. K. Inertial microfluidics-based separation of microalgae using a contraction-expansion array microchannel. *Micromachines* **12**, 97 (2021).
32. Bazaz, S. R. et al. Computational inertial microfluidics: a review. *Lab Chip* **20**, 1023–1048 (2020).
33. Tang, W. L. et al. Channel innovations for inertial microfluidics. *Lab Chip* **20**, 3485–3502 (2020).
34. Carvell, T. et al. Human leucocytes processed by fast-rate inertial microfluidics retain conventional functional characteristics. *J. R. Soc. Interface* **21**, 20230572 (2024).
35. Wu, Z. et al. Microalgae separation using spiral inertial microchannel. *Microfluid Nanofluid* **27**, 23 (2023).
36. Cha, H. et al. Multiphysics microfluidics for cell manipulation and separation: a review. *Lab a Chip* **22**, 423–444 (2022).
37. Bai, J.-J. et al. Dean-flow-coupled elasto-inertial focusing accelerates exosome purification to facilitate single vesicle profiling. *Anal. Chem.* **95**, 2523–2531 (2023).
38. Kwon, T., Choi, K. & Han, J. Separation of ultra-high-density cell suspension via elasto-inertial microfluidics. *Small* **17**, 2101880 (2021).
39. Amini, H., Lee, W. & Di Carlo, D. Inertial microfluidic physics. *Lab a Chip* **14**, 2739–2761 (2014).
40. Shen, F., Zhang, J., Zhang, C. C., Zhao, S. Y. & Liu, Z. M. Continuous and straightforward sorting of particles in microcavities with side outlets using inertial microfluidics. *Phys. Fluids* **37**, https://doi.org/10.1063/5.0254708 (2025).
41. Kuntaegowdanahalli, S. S., Bhagat, A. A. S., Kumar, G. & Papautsky, I. Inertial microfluidics for continuous particle separation in spiral microchannels. *Lab Chip* **9**, 2973–2980 (2009).
42. Zhou, J., Giridhar, P. V., Kasper, S. & Papautsky, I. Modulation of aspect ratio for complete separation in an inertial microfluidic channel. *Lab Chip* **13**, 1919–1929 (2013).
43. Warkiani, M. E. et al. Ultra-fast, label-free isolation of circulating tumor cells from blood using spiral microfluidics. *Nat. Protoc.* **11**, 134–148 (2016).
44. Chung, A. J. A minireview on inertial microfluidics fundamentals: Inertial particle focusing and secondary flow. *BioChip J.* **13**, 53–63 (2019).
45. Gao, H., Zhou, J., Naderi, M. M., Peng, Z. & Papautsky, I. Evolution of focused streams for viscoelastic flow in spiral microchannels. *Microsyst. Nanoeng.* **9**, 73 (2023).
46. Akbarnataj, K., Maleki, S., Rezaeian, M., Haki, M. & Shamloo, A. Novel size-based design of spiral microfluidic devices with elliptic configurations and trapezoidal cross-section for ultra-fast isolation of circulating tumor cells. *Talanta* **254**, 124125 (2023).
47. Lu, S., Ma, D. & Mi, X. A high-throughput circular tumor cell sorting chip with trapezoidal cross section. *Sensors* **24**, 3552 (2024).
48. Sadeghi, Z., Esfahany, M. N., Salehi, H. & Baradaran, A. Clinical isolation of breast cancer Circulating Tumor Cells with an inertial microfluidic chip with a trapezoidal cross-section. *Biochem. Eng. J.* **221**, 109788 (2025).
49. Hill, C., Willoughby, N. & Bridle, H. Efficient high-concentration dewatering of Chlorella vulgaris utilising spiral inertial microfluidics. *Bioresour. Technol. Rep.* **18**, 101014 (2022).
50. Karimi, A. & Sattari-Najafabadi, M. Numerical study of bacteria removal from microalgae solution using an asymmetric contraction-expansion microfluidic device: a parametric analysis approach. *Heliyon* **9**, https://doi.org/10.1016/j.heliyon.2023.e20380 (2023).
51. Wang, Z. et al. Enhanced particle focusing and sorting by multiple sheath stream in contraction–expansion microchannel. *Microfluid Nanofluid* **27**, 16 (2023).
52. Bagi, M. et al. Advances in technical assessment of spiral inertial microfluidic devices toward bioparticle separation and profiling: a critical review. *BioChip J.* **18**, 45–67 (2024).
53. Al-Ali, A., Waheed, W., Abu-Nada, E. & Alazzam, A. A review of active and passive hybrid systems based on Dielectrophoresis for the manipulation of microparticles. *J. Chromatogr. A* **1676**, 463268 (2022).
54. Diao, K., Zhou, T., Du, J. J., Xu, Y. H. & Zhang, D. H. Preparation of high-toughness PAM-Gel/CNTs-RGO hydrogel and its electromagnetic shielding properties. *N. J. Chem.* **48**, 19325–19336 (2024).
55. Kutluk, H., Viefhues, M. & Constantinou, I. Integrated microfluidics for single-cell separation and on-chip analysis: novel applications and recent advances. *Small Sci.* **4**, 2300206 (2024).
56. Lu, Q., Zhang, Z. & Ding, X. Isolation techniques of micro/nano-scaled species for biomedical applications. *Adv. Sci.* **12**, 2414109 (2025).
57. Shi, R., Yue, Y., Liu, Z., Chai, H. & Miao, P. Recent advances in integrated biophysical and biochemical microfluidic methods for circulating tumor cells isolation and analysis. *Fundamental. Res.* https://doi.org/10.1016/j.fmre.2024.09.010 (2024).
58. Song, Y., Li, D. & Xuan, X. Recent advances in multimode microfluidic separation of particles and cells. *Electrophoresis* **44**, 910–937 (2023).
59. Xiang, N. & Ni, Z. Inertial microfluidics: current status, challenges, and future opportunities. *Lab Chip* **22**, 4792–4804 (2022).
60. Xu, X. et al. Recent progress of inertial microfluidic-based cell separation. *Analyst* **146**, 7070–7086 (2021).
61. Xue, C. et al. Particle manipulation under X-force fields. *Lab Chip* **25**, 956–978 (2025).
62. Yan, S., Zhang, J., Yuan, D. & Li, W. Hybrid microfluidics combined with active and passive approaches for continuous cell separation. *Electrophoresis* **38**, 238–249 (2017).
63. Zhang, T. L. et al. Passive microfluidic devices for cell separation. *Biotechnol. Adv.* **71**, https://doi.org/10.1016/j.biotechadv.2024.108317 (2024).
64. Mudugamuwa, A. et al. Periodic flows in microfluidics. *Small* **20**, 2404685 (2024).
65. Xiang, N. et al. Precise size-based cell separation via the coupling of inertial microfluidics and deterministic lateral displacement. *Anal. Chem.* **91**, 10328–10334 (2019).
66. Tottori, N. & Nisisako, T. Particle/cell separation using sheath-free deterministic lateral displacement arrays with inertially focused single straight input. *Lab Chip* **20**, 1999–2008 (2020).
67. Tanaka, T. et al. Separation of cancer cells from a red blood cell suspension using inertial force. *Lab Chip* **12**, 4336–4343 (2012).
68. Moon, H. S. et al. Continual collection and re-separation of circulating tumor cells from blood using multi-stage multi-orifice flow fractionation. *Biomicrofluidics* **7**, 014105 (2013).
69. Al-Halhouli, A. A. et al. Enhanced inertial focusing of microparticles and cells by integrating trapezoidal microchambers in spiral microfluidic channels. *Rsc Adv.* **9**, 19197–19204 (2019).
70. Shahraki, Z. H., Navidbakhsh, M. & Taylor, R. A. Coupling contraction-expansion arrays with spiral microchannels to enhance microfluidic-based particle/cell separation. *Int. J. Comput. Fluid D* **36**, 63–90 (2022).
71. Herrmann, N., Neubauer, P. & Birkholz, M. Spiral microfluidic devices for cell separation and sorting in bioprocesses. *Biomicrofluidics* **13**, 061501 (2019).
72. Magalhães, V. et al. Spiral inertial microfluidics for separation and concentration of phytoplankton. *Algal Res.* **76**, 103317 (2023).